Available online at www.sciencedirect.com
ScienceDirect
Trans. Nonferrous Met. Soc. China 34(2024) 408−422
Transactions of Nonferrous Metals Society of China
www.tnmsc.cn

Effect of non-isothermal aging on microstructure and corrosion behavior of multilayer friction surfaced Al−Mg−Si alloy with Ag additive

Hamed JAMSHIDI AVAL

Department of Materials Engineering, Babol Noshirvani University of Technology, Babol 47148-71167, Iran

Received 30 May 2022; accepted 6 October 2022

Abstract: The influence of non-isothermal aging on the microstructure and corrosion behavior of multilayer friction surfaced Al−Mg−Si alloy with different amounts of silver additive was investigated. The silver in 4, 8, and 13 wt.% was inserted into the consumable rods by drilling holes in the cross-section of the consumable rods. The coating microstructure was studied by using light and electron microscopy, the mechanical properties of the coatings were studied by using microhardness and tensile tests, and the corrosion resistance of samples was studied by using electrochemical testing. The results show that the grain size of friction surfaced layers decreases from (1.5±0.3) to (1.0±0.3) μm with increasing the silver additive content from 4 to 13 wt.%. The solute silver in the aluminum matrix increases the precipitation kinetics in the Al−Mg−Si alloy. After non-isothermal aging, the yield and tensile strengths of the silver-containing coating are 50.6% and 43.5% higher than those of the silver-free coating, respectively. Non-isothermal aging treatment reduces corrosion current density and increases corrosion resistance of both samples with and without silver additive. The corrosion resistance of the silver-containing coating after non-isothermal aging is 96.5% higher than that of the silver-free coating.

Key words: non-isothermal aging; microstructure; corrosion behavior; Al−Mg−Si alloy; silver additive; multilayer friction surfacing

1 Introduction

Studies have shown that the addition of silver to precipitation hardenable aluminum alloys will lead to a significant change in the precipitation sequence of these alloys [1]. The presence of silver with magnesium is more effective in the precipitation process of the alloy. In fact, silver accelerates the nucleation and growth of strengthening precipitates to achieve higher strength and hardness values in fewer periods of heat treatment. Research has shown that silver in limited amounts (for example, 0.3 at.% in Al−Zn−Mg alloys) will have a significant effect on the precipitation process. Higher amounts of silver will lead to the formation of silver-rich secondary phase particles, which causes the activation of other strengthening mechanisms in addition to the strengthening mechanism through precipitates. The effect of silver addition on Al−Zn−Mg [1,2] and Al−Cu−Mg [3] alloy systems has been studied by various researchers. However, the effect of silver addition on the Al−Mg−Si alloy system has been studied in a limited way.

Although the main research about the effect of silver on the precipitation behavior of aluminum alloys was done based on isothermal aging heat treatment, studies have shown that one of the solutions to simultaneously improve the mechanical properties and corrosion resistance of precipitation hardenable aluminum alloys is non-isothermal aging (NIA) heat treatment instead of isothermal aging heat treatment of precipitation hardenable

Corresponding author: Hamed JAMSHIDI AVAL, Tel: +98-11-35501800, Fax: +98-11-35501808, E-mail: h.jamshidi@nit.ac.ir
DOI: 10.1016/S1003-6326(23)66407-6

aluminum alloys [4−6]. Although various conditions of the isothermal aging process have been extensively investigated [7−11], the NIA studies on Al−Zn−Mg−Cu [4,12−15], Al−Mg−Si [16−18] and Al−Cu−Mg−Si [19] alloy systems have shown that the NIA treatment increases the corrosion resistance by reducing the precipitate-free zone (PFZ) and the precipitate aggregation at the grain boundary. It was also reported that the tensile and yield strengths of the alloy significantly increased after NIA treatment compared to those after isothermal aging heat treatment [20−23]. It has also been reported in some sources that the initial precipitates formed during NIA treatment prevent dynamic recovery during the deformation or static recovery in the early annealing stage.

Despite the existence of conventional methods in the manufacture of aluminum alloy, recent studies have shown that heat and severe plastic deformation applied along with severe plastic deformation processes such as friction stir processing [24] and friction surfacing [25,26] can cause the dissolution of additive elements and thus alloying in the processed material. Although studies have shown that the recovery rate of additives and their dissolution in the matrix depend on the process parameters, most of the additives are remained in the form of secondary phase particles in the matrix and led to the activation of the strengthening mechanism through particles. The friction surfacing process is known as a tool for applying metal coatings on similar and dissimilar metal substrates. However, the high capability of this process in applying a fine-grained layer with significant mechanical and tribological properties compared to other coating processes based on consumable melting has prompted research into the ability of this process to additive manufacturing of various structures and alloys. DILIP et al [27] studied the application of multilayer coatings by using the friction surfacing method. They reported that the fabrication of plain carbon steel multilayer coatings using the friction surfacing process resulted in the formation of an integrated fine-grained structure with a strong bond between various layers. In another study, DILIP and JANAKI RAM [28] investigated the AA2014 aluminum alloy multilayer coating on AA5083 aluminum alloy substrate. They reported that the use of the consumable rod in the T6 treatment leads to over aging in the applied coatings. Although the loss of strength can be eliminated by solution treatment and aging of the coatings, this treatment causes extensive grain growth in the coating. GANDRA et al [29] studied the fabrication of AA6082−SiC composite gradient coating on AA2024 aluminum alloy substrate. By using the friction surfacing process, they applied a multilayer coating with a gradual change in SiC content from 5 to 30 wt.%. They showed that despite the occurrence of over aging in the substrate, the hardness of the last layer increased by 30% compared to that of the coating without reinforcement.

According to the available sources, the effect of non-isothermal aging heat treatment on Al−Mg−Si alloys containing silver has not been investigated so far. In this research, by applying a friction-surfaced multilayer coating of Al−Mg−Si alloy containing different amounts of silver on AA2024 aluminum alloy substrate, the effect of non-isothermal aging heat treatment on the microstructure, mechanical properties, and corrosion resistance of the applied coating was investigated.

2 Experimental

In order to apply the Al−Mg−Si alloy multilayer coating on the AA2024 aluminum alloy substrate, AA6061 aluminum alloy consumable rod with chemical composition of 0.62% Si, 0.57% Fe, 0.32% Cu, 0.11% Mn, 1.15% Mg, and Al balance, and AA2024 aluminum alloy sheet with chemical composition of 0.18% Si, 0.25% Fe, 3.21% Cu, 0.40% Mn, 1.35% Mg, and Al balance (all in wt.%) were prepared. The substrate was 2 mm in thickness and the consumable rod was 20 mm in diameter. The consumable rods with a length of 10 cm and a substrate with dimensions of 10 cm × 10 cm were cut. As shown in Fig. 1, according to the previous research [30], in order to apply silver powder in 4, 8, and 13 wt.%, holes with diameters of 2.5, 3.5, and 4.5 mm were drilled in the cross-section of the consumable rod. Figure 2 shows transmission electron microscopy (TEM) image of silver nano powder used in this study. As shown in Fig. 2, the silver powder, with an average size of (15±7) nm, was used as the additive. All consumable rods used were solid-solutionized before coating. The rods were treated at 530 °C for 2 h, and then quenched in

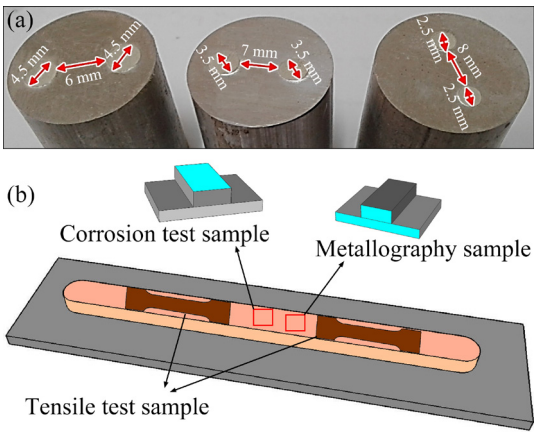

Fig. 1 Holes drilled in cross-section of consumable rods (a), and schematic illustration of microstructural examination, corrosion test, and tensile test extraction position (b)

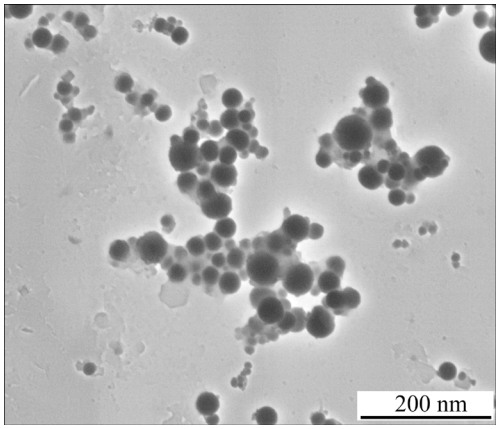

Fig. 2 TEM image of silver nanopowder used in this study

water. All coatings were measured at a rotational speed of 800 r/min, a traverse speed of 100 mm/min, and an axial feeding rate of 125 mm/min. In order to compare the multilayer coating containing silver powder and the coating without silver, a multilayer coating was applied using the same parameters but with a consumable rod without silver additive. In order to investigate the effect of NIA treatment after coating, the multilayer samples containing silver powder, without silver powder, and substrate were first solid-solutionized at 530 °C for 8 h. Then, the solutionized samples were subjected to non-isothermal aging treatment with a heating rate of 10 °C/min.

After coating operation, different samples were extracted for microstructural studies, mechanical properties test, and corrosion evaluation of coatings. In order to study the precipitation sequence during non-isothermal heat treatment, differential scanning calorimetry (DSC) test samples were extracted from two coatings. The samples were then subjected to a heating rate of 10 °C/min in N_2 atmosphere using a DSC 204 Phoenix. The microstructure of the coated samples was studied using optical and scanning electron microscopes. The hardness of the samples was measured using the micro-Vickers hardness test according to the ASTM E92 standard with a load of 100 g for a duration of 10 s. According to Fig. 1, tensile test samples were prepared from samples with and without silver powders. The tensile test was performed with a cross-head speed of 1 mm/min. In order to investigate the corrosion behavior of the samples, the corrosion test was performed by IVIUM model Vertex using a solution of 3.5 wt.% NaCl as a corrosion medium. In the corrosion test, a saturated calomel electrode was used as a reference electrode and platinum as an auxiliary electrode. The scanning rate of 1 mV/s was used in all experiments. Before starting the test and drawing the TOEFL curve, in order to reach steady state condition, all samples were immersed in a 3.5 wt.% NaCl solution for 30 min.

3 Results and discussion

3.1 Macrostructure

The cross-sections of coated samples without and containing silver powder are shown in Fig. 3. The coating efficiency ($\eta_{coating}$) was calculated according to the procedure reported in Ref. [31] as follows:

$$\eta_{coating}=\frac{A_d v W_b}{\pi r^2 v_z W_d} \quad (1)$$

where A_d is the deposited cross-section area, v is the traverse speed of the consumable rod, W_b is the effective bonded width, πr^2 is the cross-section area of the consumable rod (r is the radius of the consumable rode), v_z is the axial feeding rate, and W_d is the maximum coating width. Coating efficiencies of Layers 1, 2, and 3 in the sample containing silver were 17%, 19%, and 20%, respectively. The coating efficiencies of Layers 1, 2, and 3 in the sample without silver was 15%, 18%, and 19%, respectively. The higher efficiency of the coating in different layers of the sample containing silver powder and its increase with increasing the

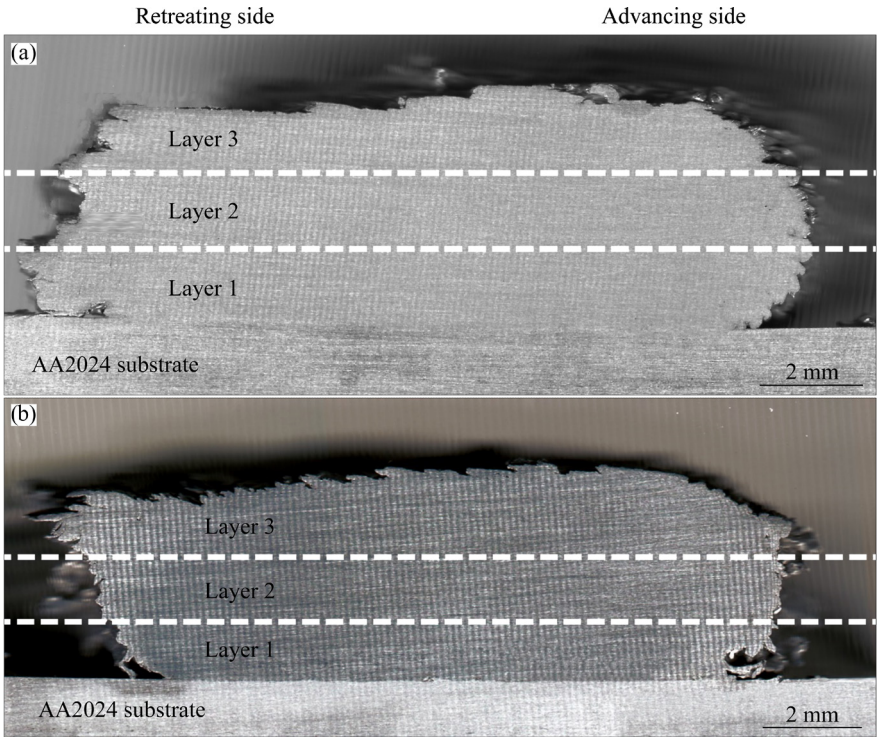

Fig. 3 Cross-sections of coated samples: (a) Sample containing silver; (b) Sample without silver (The silver powder content of Layers 1, 2, and 3 in the sample is 4, 8, and 13 wt.%, respectively)

amount of silver powder are related to the change of friction conditions on the contact surface of the consumable rod. As the consumable rods are in solid solution condition during the process due to heat and plastic deformation, it is possible to increase the strength of the consumable rod. Therefore, it is expected that by reducing the heat input during the process, a smaller increase in the strength of the consumable rod will occur. By reducing the strength of the consumable rod, the amount of plastic deformation increases during the process, and as a result, the material deposition on the substrate will increase during the surfacing. By applying a hole in the cross-section of the consumable rod, a part of the consumable rod material is removed, which reduces the amount of friction and thus reduces the heat input. As the heat input decreases, the strength of the consumable rod decreases and the plastic deformation capability of the consumable rod increases, which increases the deposition rate and the efficiency of the coating. Temperature measurements in various areas of the silver powder-containing sample revealed that the temperatures at the substrate/Layer 1, Layer 1/ Layer 2, and Layer 2/Layer 3 interfaces are 391, 379, and 368 °C, respectively. The decrease in temperature by increasing the mass fraction of silver in the consumable rod confirms the claim of reducing the heat input due to the drilling of holes in the consumable rod. On the other hand, it can be seen that the efficiency of the coating in different layers does not differ much in the sample without silver powder. Although no noticeable temperature difference is observed at the interface of substrate/ Layer1, Layer 1/Layer 2, and Layer 2/Layer 3 of the sample without silver powder (398, 396, and 392 °C, respectively), the decrease in coating temperature with an increasing number of layers is probably related to the effect of the underlying layers and the increase in heat sink caused by these layers. A comparison of the efficiency results obtained in this study with the values reported in Ref. [30] shows that solid solution treatment has a strong impact on the coating efficiency process. In fact, the solid solution treatment reduces the efficiency of the coating in the sample without silver powder compared to the conditions in which the aged rod is used.

3.2 Microstructure before heat treatment

Figure 4 shows the microstructures in the center zone of different layers of silver-containing

and silver-free samples before heat treatment. Also, the microstructures on the advancing and retreating sides of different layers of silver-containing and silver-free samples are shown in Figs. 5 and 6, respectively. Irrespective of the presence or absence of silver, the grain size on the advancing side, retreating side, and in the central zone of a layer is not significantly different. Also, despite the small difference in grain size of different layers in the sample without silver, in the sample containing silver, the grain size decreases with increasing the content of silver powder. Based on Ref. [32], the formation of an equiaxed microstructure in the coating is caused by the occurrence of a dynamic recrystallization mechanism. Two factors, temperature and plastic strain rate, play a key role in the formation of the recrystallized microstructure. As the temperature decreases and the plastic strain rate

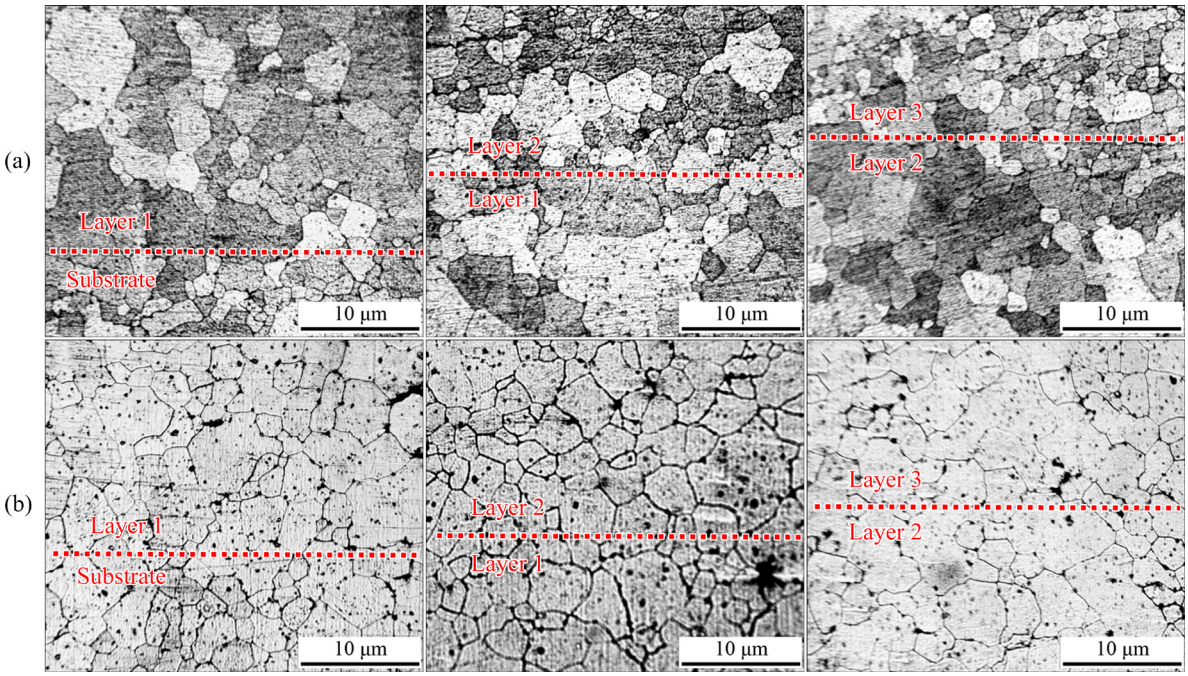

Fig. 4 Microstructures in center zone of different layers of silver-containing (a) and silver-free (b) samples before heat treatment

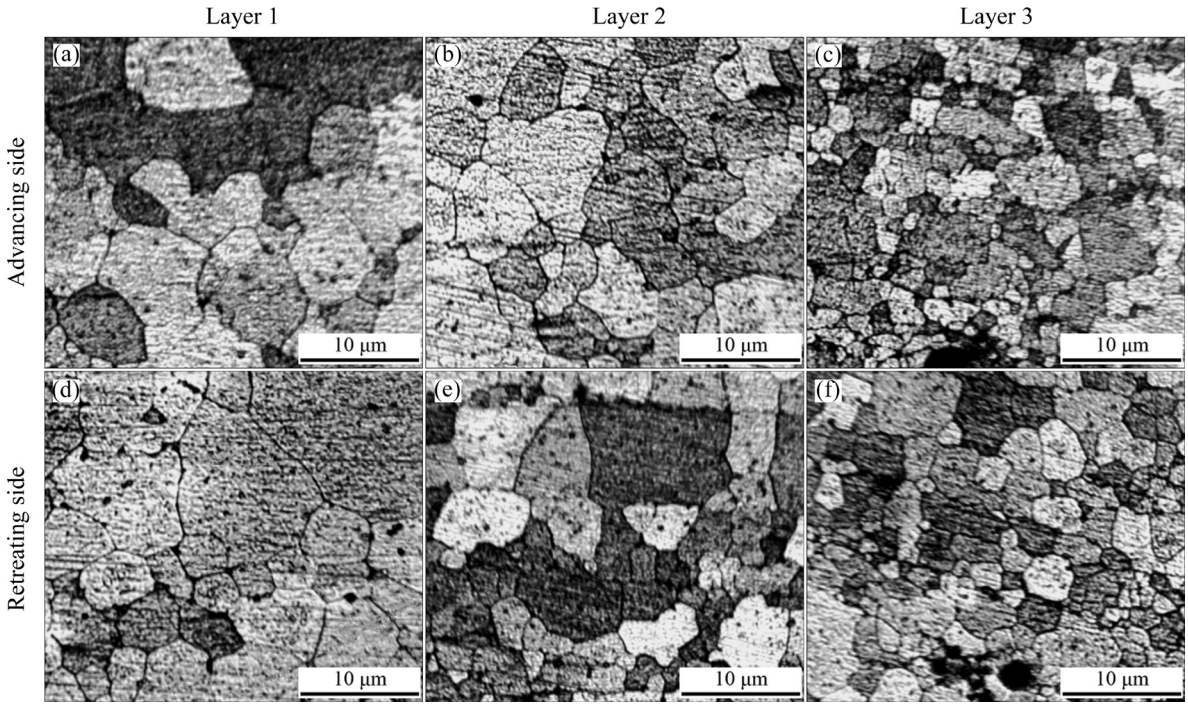

Fig. 5 Microstructures of different layers on advancing and retreating sides of silver-containing sample

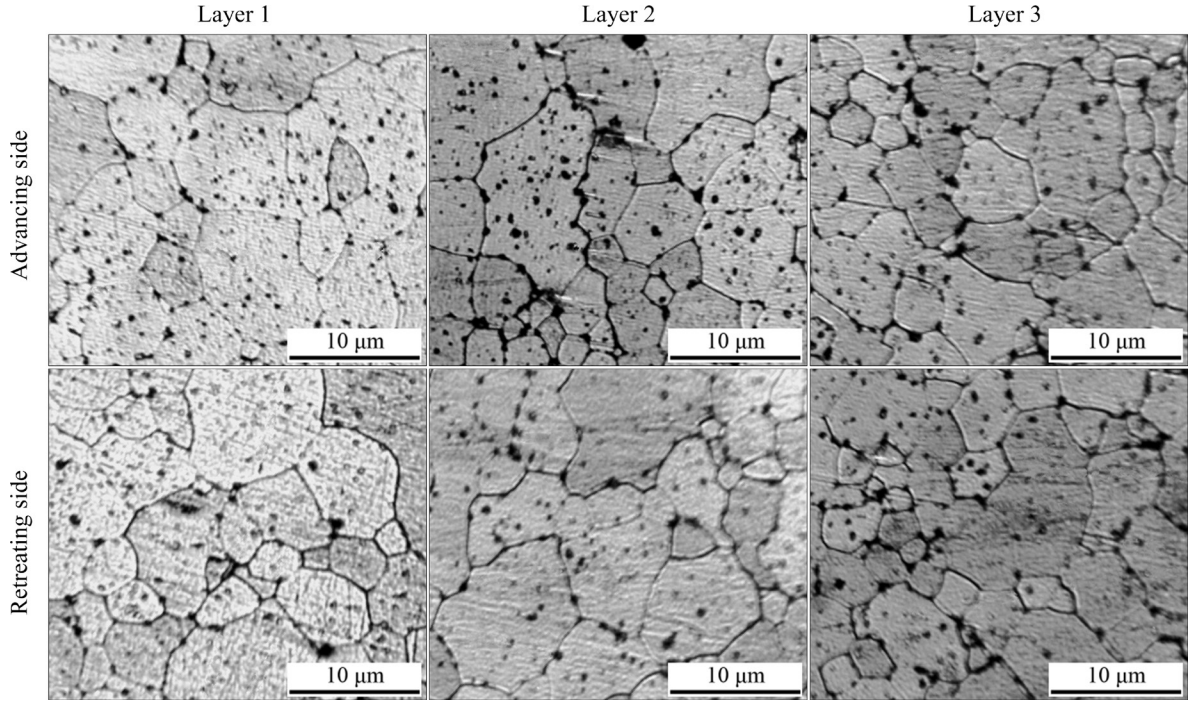

Fig. 6 Microstructures of different layers on advancing and retreating sides of silver-free sample

increases, the size of the recrystallized grain decreases. According to Refs. [33,34], the following equation can be used to estimate the plastic strain rate ($\dot{\varepsilon}$) during the coating process:

$$\dot{\varepsilon}= 2\pi n\left(\frac{dW_{\mathrm{b}}v}{\pi v_z}\right)^{0.5}\Big/ d_{\mathrm{eff}} \tag{2}$$

where n denotes the mean material flow rate, d_{eff} represents the effective thickness of the coating, and d is the coating thickness. The plastic strain rate can be obtained according to the process parameters and geometric parameters of the coating. Accordingly, the plastic strain rate of Layers 1, 2, and 3 in the sample that contains silver powder is 1236, 1249, and 1262 s^{-1}, respectively. The strain rate increases from Layer 1 to Layer 3. The temperature measurements have also shown that the temperature decreases with movement from Layer 1 to Layer 3. Therefore, both the temperature and the plastic strain rate act to reduce the grain size. Based on the results reported in Ref. [30], the use of aged consumable rod leads to similar results, meaning that with increasing the content of silver powder, grain size decreases. However, based on the results obtained from the aged rod, it was found that compared to plastic strain rate, the effect of temperature on the coating grain size is dominant. However, it should be noted that the presence of silver-rich particles activates the particle stimulated nucleation (PSN) mechanism, which can reduce the grain size of the coating by increasing the content of silver powder.

3.3 Hardness after NIA treatment

Changes in the hardness of the sample containing and without silver at different non-isothermal aging temperatures are shown in Fig. 7. In both types of coatings, the hardness first increases and then decreases with increasing aging temperature. However, the increase in hardness of the coating occurs in the sample containing silver at a lower temperature and the decrease in hardness at the maximum aging temperature in the sample containing silver powder is less. The faster increase in hardness in samples containing silver powder is related to the effect of silver on the aluminum structure and helps to increase the precipitation kinetics. On the other hand, the presence of silver-rich particles prevents a large drop in hardness at high aging temperatures. In other words, it can be said that the addition of silver by creating silver-rich secondary phase particles leads to an increase in the thermal stability of the coating. A comparison of the results of coating hardness in different layers with the values reported in Ref. [30]

shows that the use of rods in aged conditions and isothermal aging heat treatment after coating leads to lower values of hardness of the coating under similar conditions. In order to investigate the cause of different hardness changes in the sample containing and without silver powder, micro-structural changes after non-isothermal aging were studied.

3.4 Microstructure after heat treatment

Figures 8(a) and (b) show the microstructures of different layers of samples containing and without silver powder after non-isothermal aging heat treatment at temperatures of 200 and 250 °C, respectively. Also, the grain sizes of different layers at different aging temperatures are reported in Table 1. In both samples, by solid solution heat treatment, the grain growth occurs in different layers. However, it should be noted that grain growth is not very noticeable after non-isothermal aging heat treatment. Due to grain growth during the solid solution treatment of the sample containing silver, the grain sizes of different layers are almost identical to each other, and there is no noticeable difference between the grain sizes of different layers. Although grain growth occurs in both samples, the degree of grain growth in the sample without silver powder is much higher than the sample containing silver powder. Dissolution of precipitates during solid solution treatment and removal of obstacles against the movement of grain boundaries are the important reasons for significant grain growth in silver-free samples. Although precipitate dissolution also occurs in the sample containing silver, silver-rich

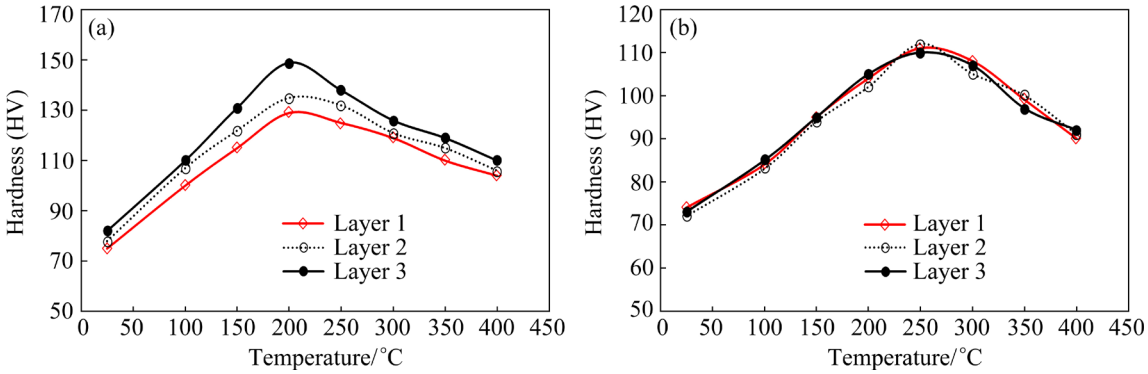

Fig. 7 Variation of average hardness versus NIA treatment temperature of silver-containing (a) and silver-free (b) samples

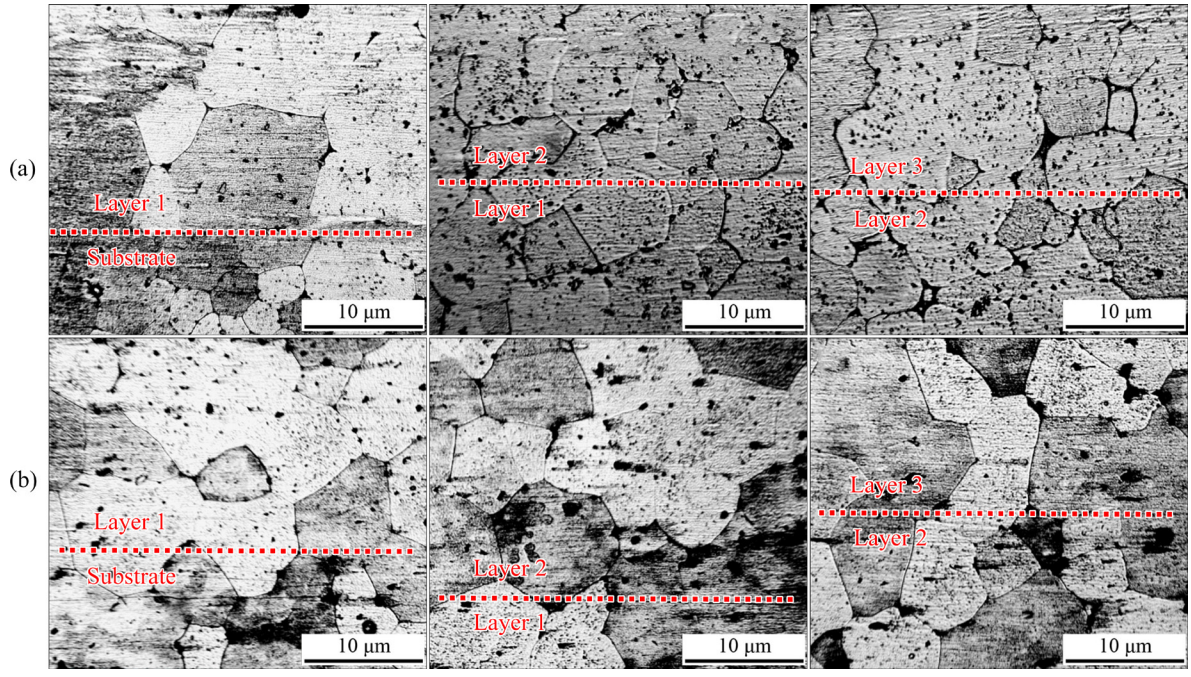

Fig. 8 Microstructures of different layers in different samples: (a) Silver-containing sample after NIA treatment at 200 °C; (b) Silver-free sample after NIA treatment at 250 °C

particles act as grain boundary locking agents and prevent excessive grain growth in the sample containing silver powder during heat treatment. The comparison of microstructural results with the results reported in Ref. [30] shows that similar results are observed after isothermal heat treatment of samples coated with and without silver powder. Researchers in Ref. [30] reported that due to the silver-rich particles hindering grain boundary movement, no significant difference was observed in the grain size of different layers of silver-containing coating.

3.5 Precipitates evolution before and after heat treatment

SEM images of the sample containing and without silver powder before and after the non-isothermal aging treatment are shown in Figs. 9 and 10, respectively. In the sample without silver powder in all layers before heat treatment, the microstructure contains $\beta(Mg_2Si)$ and Si-rich precipitates and secondary phase particles. Moving from Layer 1 to Layer 3, the difference in precipitate size is not noticeable. After heat treatment, the size of the $\beta(Mg_2Si)$ precipitates becomes smaller, but the size of the Si-rich secondary phase particles does not change much. In the sample containing silver powder before heat treatment, $\beta(Mg_2Si)$, Si-rich, and silver-rich precipitates and secondary phase particles are observed in the structure. The $\beta(Mg_2Si)$ precipitate size is finer compared to that of samples without silver powder. The reduction in size of the precipitates is related to the lower heat input during

Table 1 Grain sizes of different layers of coatings containing and without silver at different NIA treatment temperatures

Coating	Layer No.	Grain size/μm							
		400 °C	350 °C	300 °C	250 °C	200 °C	150 °C	100 °C	25 °C
Silver-free	1	11.4±0.4	10.8±0.2	11.1±0.1	11.2±0.3	10.8±0.6	11.2±0.5	10.9±0.5	11.3±0.6
	2	11.2±0.1	11.3±0.6	10.9±0.7	11.1±0.6	10.9±0.3	11.5±0.1	11.2±0.3	11.5±0.2
	3	11.5±0.6	11.2±0.5	11.2±0.5	10.9±0.6	11.2±0.5	11.2±0.1	11.5±0.6	11.8±0.3
Silver-containing	1	10.2±0.3	9.9±0.5	9.9±0.2	9.9±0.3	10.1±0.3	9.8±0.7	10.1±0.3	9.9±0.4
	2	10.5±0.1	9.8±0.2	9.8±0.8	9.9±0.5	10.6±0.6	9.9±0.5	10.2±0.2	10.1±0.3
	3	9.9±0.3	10.1±0.1	10.2±0.3	10.1±0.7	10.3±0.4	10.2±0.4	9.9±0.5	10.4±0.6

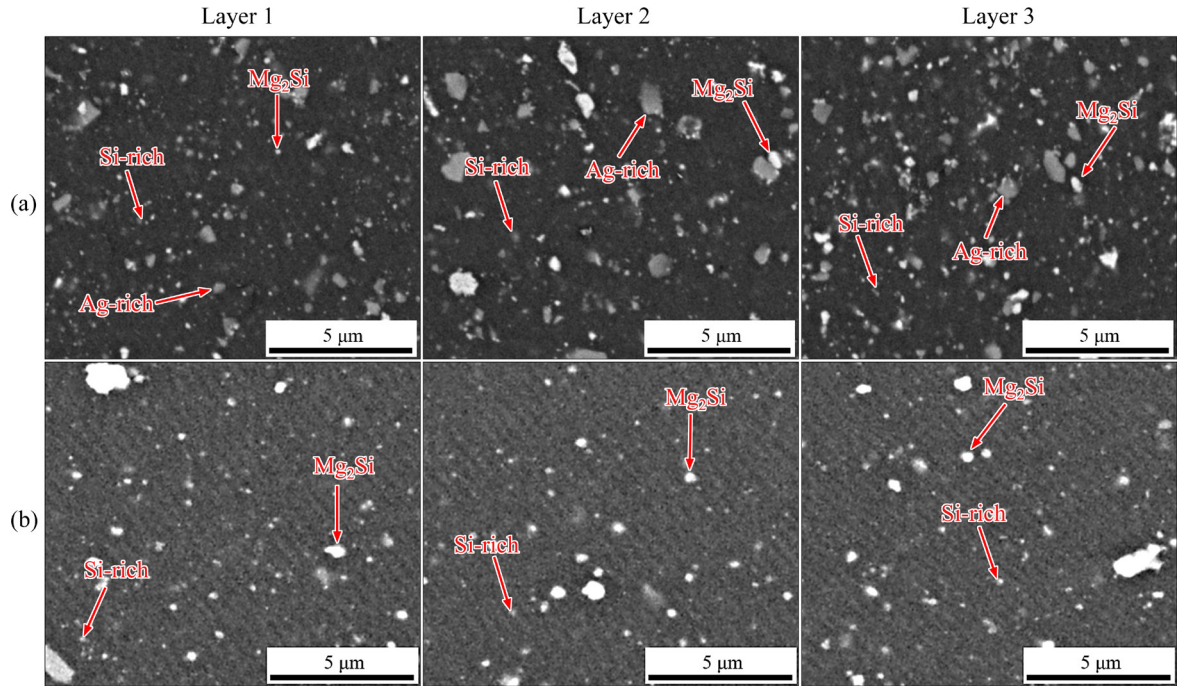

Fig. 9 Microstructures of different layers in different samples before NIA treatment: (a) Silver-containing sample; (b) Silver-free sample

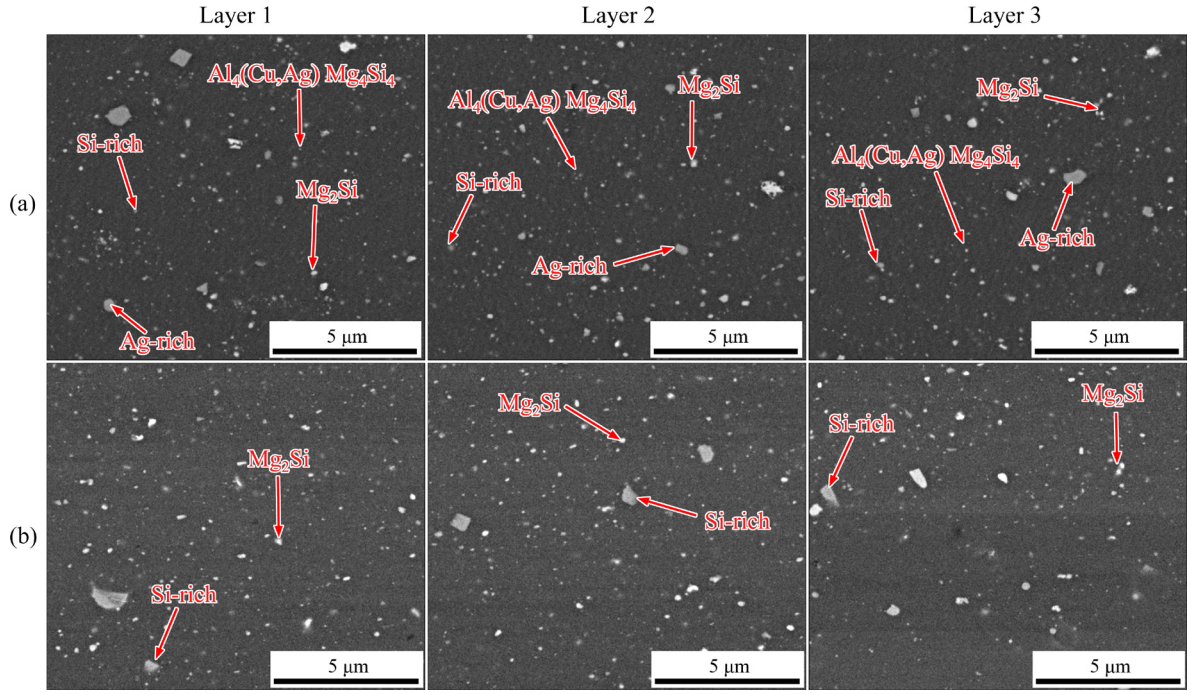

Fig. 10 Microstructure of different layers in different samples after NIA treatment: (a) Silver-containing sample; (b) Silver-free sample

the coating of the layers containing silver powder, which prevents the growth of these precipitates, and finer precipitates are formed in the structure than in the sample without silver powder. It should be noted that higher heat input during coating of a sample without silver powder leads to a more complete precipitation process in solid-solutionized rods. As a result, it can be expected that by increasing the heat input, the precipitates will be fully formed and the growth stage of the precipitates will begin. After non-isothermal heat treatment, the size of Mg_2Si precipitates decreases, as in the case without silver powder. After non-isothermal heat treatment in the silver-containing sample, the Q ($Al_4(Cu,Ag)Mg_4Si_4$) precipitates are formed. The presence of smaller silver-rich particles is quite evident after the aging treatment. The reason for this is the solid solution treatment and the possibility of silver dissolution in the aluminum matrix.

In order to study the precipitation sequence of samples containing and without silver, after solid solution treatment, the DSC samples were prepared from Layers 1−3 of different coated samples. The DSC test results are shown in Fig. 11. As can be seen, the precipitation sequences of the two coatings are not much different, and the only

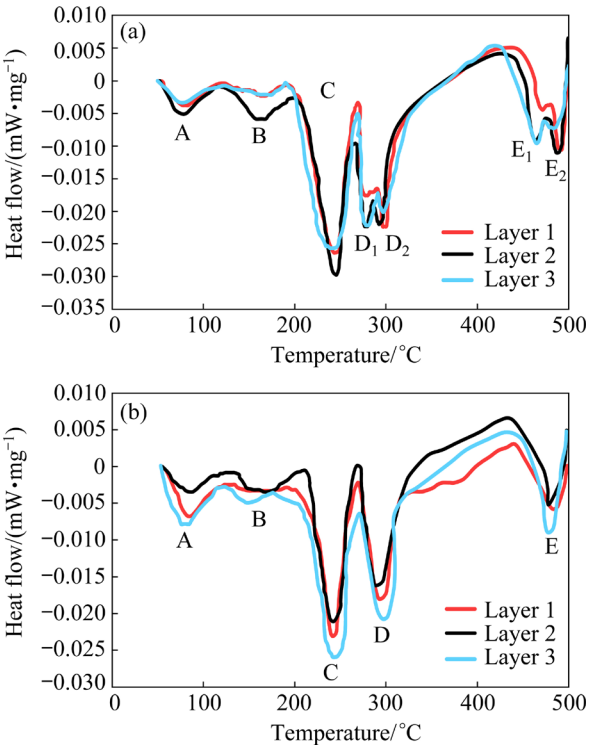

Fig. 11 DSC data of different layers in different samples: (a) Silver-containing sample, (b) Silver-free sample

obvious difference between the two coatings is the height and position of the peaks related to different precipitation stages. By comparing data reported in Refs. [35−37], in the coating without silver, the

exothermic peaks around 80 °C (Peak A) and in the temperature range of 120−190 °C (Peak B) are related to the formation of vacancy−Si clusters and GP zone, and peaks around 240 °C (Peak C) and 290 °C (Peak D) are related to the formation of β'' and β' precipitates, and the exothermic peak around 480 °C (Peak E) is related to the formation of β precipitates. In the silver-containing coating, Peaks D_1 and D_2 are related to the formation of β' and Q' precipitates. Also, Peaks E_1 and E_2 are related to the formation of β and Q precipitates. As can be seen, with the addition of silver powder, the heights of peaks related to Q' and Q precipitates increase. This indicates that the addition of silver to the aluminum matrix increases the precipitation rate of Q ($Al_4(Cu,Ag)Mg_4Si_4$) precipitates.

3.6 Tensile test results of coated samples

The results of the tensile test samples containing and without silver powder before and after non-isothermal heat treatment are shown in Fig. 12. The results show that by performing the aging heat treatment, the yield strength and tensile strength of both samples increase, but the elongation decreases. It should be noted that the increase rate in strength of the sample containing silver powder is much higher than that of the sample without silver powder. Indeed, after non-isothermal aging, the yield and tensile strengths are 19.4% and 3.6% higher respectively than those of the sample without silver powder. Although the two samples do not differ much in the nature and morphology of the precipitates, the presence of silver-rich particles by activating the strengthening mechanism through secondary phase particles could be the main reason for the higher strength in the sample containing silver powder. Figure 13 shows the fracture surface of different layers in the samples containing and without silver powder after non-isothermal aging treatment. In the sample without silver powder, the presence of smaller and deeper dimples in Layer 1 indicates a greater elongation of this layer. After addition of silver powder, the dimples become shallower, which is consistent with the results of the stress−strain curve. On the other hand, dimples in the sample containing silver powder after non-isothermal heat treatment are less than those in the sample without silver powder.

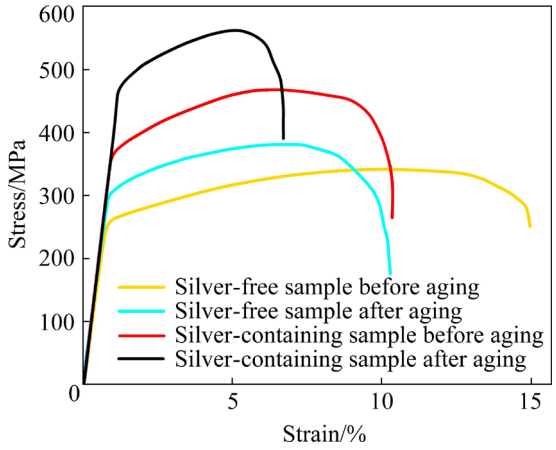

Fig. 12 Stress−strain curves of silver-free and silver-containing samples before and after NIA treatment

3.7 Corrosion behavior

The pitting morphologies of silver-containing, silver-free samples, and substrate, are shown in Fig. 14. The substrate has a larger number of pits with smaller size than silver-containing and silver-free samples. The pits on the substrate are linearly concentrated in localized regions. The semi-linear distribution of pits should be due to the elongated grains induced by rolling processing, suggesting a preferential corrosion feature at grain boundaries. It is observed that the sample without silver presents larger and deeper pits than that containing silver. The larger average size of pits in the sample without silver is because the larger Mg_2Si and Si-rich precipitates and secondary phase particles are more easily pitted. The important point is that the presence of silver-rich particles in the silver-containing sample along with finer secondary phase particles and precipitates leads to the reduction in the amount of corrosion on the surface.

Figure 15 shows potentiodynamic polarization curves of substrate and different coated samples after non-isothermal aging treatment. It should be noted that the corrosion potential can be considered as the necessary force for the corrosion reaction to occur. Therefore, the more positive the corrosion potential is, the greater force is needed to perform the corrosion. On the other hand, the corrosion current density means the amount of charge exchanged in the corrosion reaction, therefore, the lower the quantity, the higher the corrosion resistance of the sample. The corrosion started by attacking Cl^- ions on the oxide surface, as the test was conducted in NaCl. The Cl^- ions are replaced

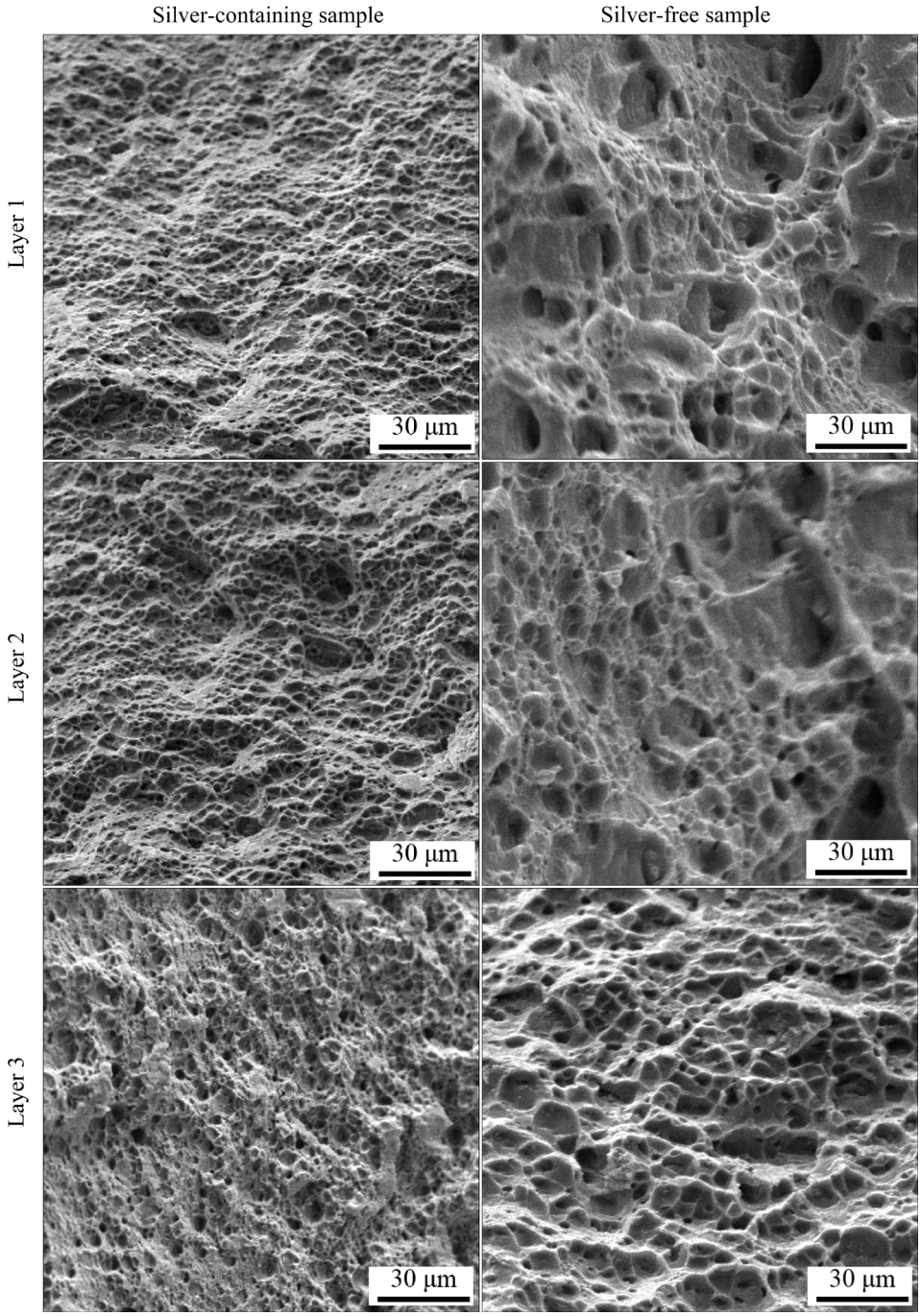

Fig. 13 SEM images showing fracture surfaces of different layers in silver-free and silver-containing samples after non-isothermal heat treatment

by oxygen in the uniform oxide film and chlorine metal is formed, which reduces the oxide film and begins to form cavities. Thus, corrosion products mainly containing aluminum hydroxide ($Al(OH)_3$), aluminum oxide (Al_2O_3) and aluminum chloride ($AlCl_3$) have been observed [35]. According to Fig. 15, it is clear that the use of silver powder leads to the transfer of polarization curves to more positive potentials and lower current densities. Also, the values of corrosion potential and corrosion current densities obtained from the potentiodynamic polarization curves are reported in Table 2. On the other hand, it is observed that the coated samples have higher corrosion resistance than the AA2024 aluminum substrate. According to Table 2, it is clear that the corrosion potential of silver-containing and silver-free samples is 3.2% and 1.7% less than that of the substrate, respectively, and the corrosion current density is 99.5% and 86.8% less than that of the substrate, respectively. Corrosion current

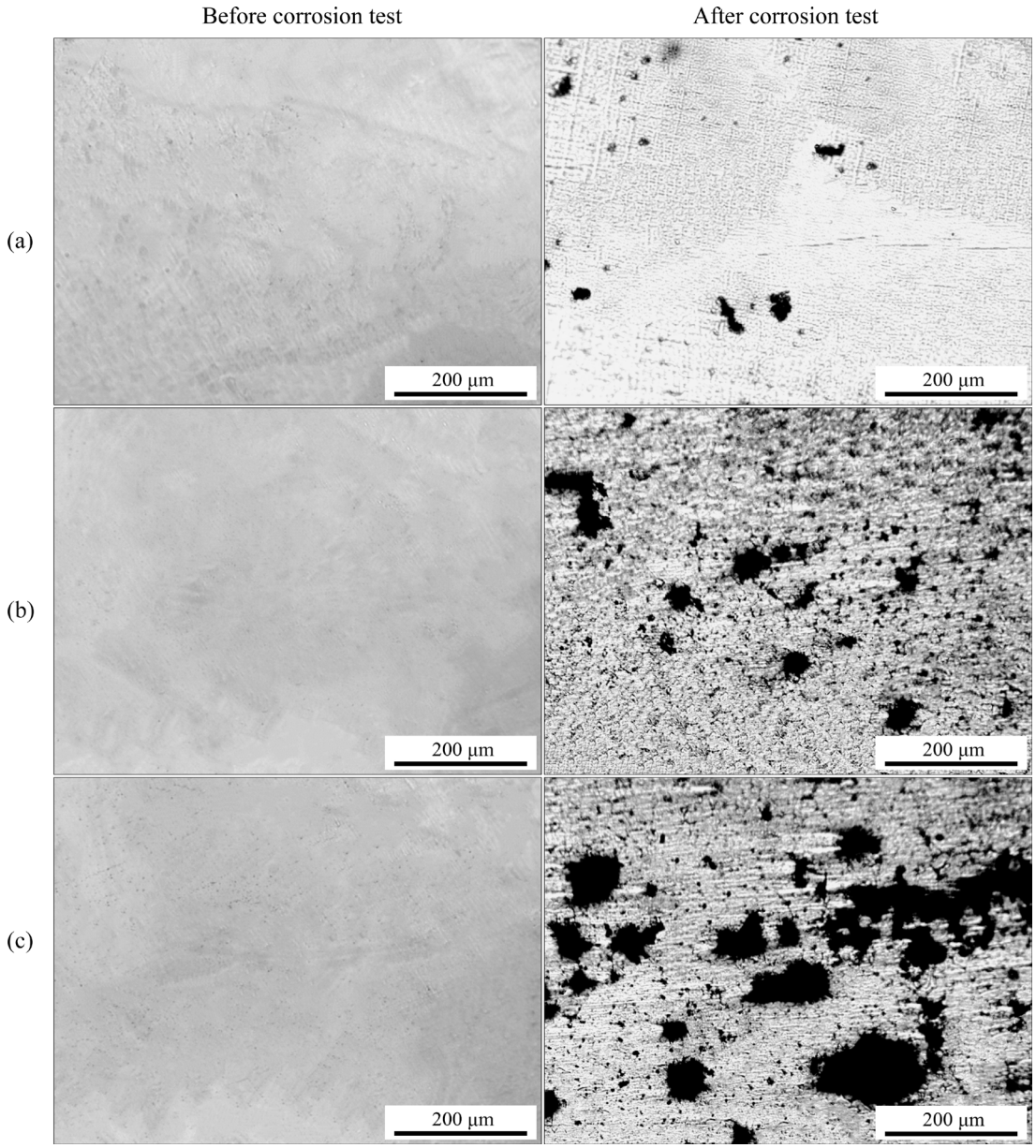

Fig. 14 Surface morphologies of different samples before and after corrosion test: (a) Silver-containing sample; (b) Silver-free sample; (c) Substrate

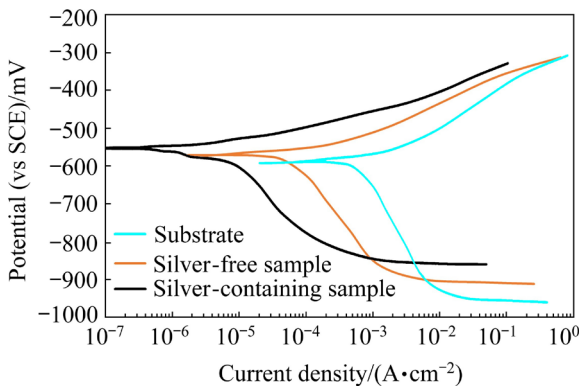

Fig. 15 Polarization curves of substrate, silver-free and silver-containing samples after NIA treatment

Table 2 Electrochemical parameters of different samples

Sample	φ_{corr} (vs SCE)/mV	J_{corr}/(mA·cm^{-2})
Silver-containing	−556.64	0.011
Silver-free	−565.11	0.315
Substrate	−575.01	2.402

density is 2.402, 0.315, and 0.011 mA/cm^2 for the substrate, silver-free, and silver-containing samples, respectively. All these results clearly indicate the positive effect of adding silver on the corrosion resistance of AA6061 aluminum alloy. The increased corrosion resistance in the silver-containing samples

can be related to smaller grain size and the presence of silver-rich particles. Reducing the grain size due to the friction surfacing process means increasing the grain density in the metal. Therefore, as grain boundaries tend to have a higher chemical reaction than other areas, it is expected that the process of protective surface layer formation is facilitated. Another important point is the finer size of β and Q precipitates in the sample containing silver powder, which leads to an increase in corrosion resistance. The comparison of corrosion results with the results reported in Ref. [30] shows that non-isothermal heat treatment reduces corrosion density and increases corrosion resistance in both samples with and without silver powder. The smaller grain size as well as the silver-rich secondary phase particles in the samples subjected to non-isothermal heat treatment can be the main reasons for the increase in corrosion resistance.

4 Conclusions

(1) Although the coating efficiency increases by increasing silver additive in different layers, the efficiency of the coating in different layers does not differ much in the sample without silver additive.

(2) Irrespective of the presence or absence of a silver additive, the grain size on the advancing side, retreating side, and in the central zone of a layer is not significantly different.

(3) In the sample containing silver, the increase in hardness of the coating occurs at a lower temperature and also the decrease in hardness at the maximum aging temperature in the sample containing silver powder is less. The presence of silver-rich particles prevents a large drop in hardness at high aging temperatures and increases the thermal stability of the coated layers.

(4) In both samples containing and without silver, by solid solution heat treatment after friction surfacing, the grain growth occurs in different layers. However, the grain growth is not very noticeable after non-isothermal aging heat treatment.

(5) The corrosion potential of silver-containing and silver-free samples is 3.2% and 1.7% less than that of the substrate, respectively, and the corrosion current density is 99.5% and 86.8 % less than that of the substrate, respectively.

(6) The smaller grain sizes as well as the silver-rich secondary phase particles in the samples that have been subjected to non-isothermal heat treatment can be the main reasons for the increase in corrosion resistance.

References

[1] POLMEAR I J. The influence of small additions of silver on the structure and properties of aged aluminum alloys [J]. JOM, 1968, 20(6): 44−51.

[2] ZHANG K, LIU Z Y, FENG C. The effect of small addition of silver on the microstructure and mechanical properties of a high-zinc super-high strength aluminum alloy [J]. The Chinese Journal of Nonferrous Metals, 2005, 15(1): 116−122. (in Chinese)

[3] AULD J H, VIETZ J T, POLMEAR I J. *T*-phase precipitation induced by the addition of silver to an aluminium–copper–magnesium alloy [J]. Nature, 1966, 209(5024): 703−704.

[4] LI Y, XU G F, PENG X Y, LIU S C, DENG Y, LIANG X P. Effect of non-isothermal aging on microstructure and properties of Al−5.87Zn−2.07Mg−2.42Cu alloys [J]. Transactions of Nonferrous Metals Society of China, 2021, 31(10): 2899−2908.

[5] FARAJOLLAHI R, JAMSHIDI AVAL H, JAMAATI R. Non-isothermal aging behavior of in-situ AA2024−Al_3NiCu composite [J]. Transactions of Nonferrous Metals Society of China, 2022, 32(7): 2125−2137.

[6] HUA L, YUAN P G, ZHAO N, HU Z L, MA H J. Microstructure and mechanical properties of 6082 aluminum alloy processed by preaging and hot forging [J]. Transactions of Nonferrous Metals Society of China, 2022, 32(3): 790−800.

[7] WANG Y C, WU X D, YUE L, GUO M X, CAO L F. Aging precipitation behavior and properties of Al−Zn−Mg−Cu−Zr−Er alloy at different quenching rates [J]. Transactions of Nonferrous Metals Society of China, 2022, 32(4): 1070−1082.

[8] TANG L, PENG X Y, JIANG F Q, LI Y, XU G F. Strong and ductile Al−Zn−Mg−Zr alloy obtained by equal angular pressing and subsequent aging [J]. Transactions of Nonferrous Metals Society of China, 2022, 32(5): 1428−1441.

[9] BAKHSHI R, FARSHIDI M H, SAJJADI S A. Strengthening of aluminium alloy 7005 through imposition of severe plastic deformation supplemented by different ageing treatments [J]. Transactions of Nonferrous Metals Society of China, 2021, 31(10): 2909−2921.

[10] WU X, HAN F, WANG W W. Effects of solution treatment and aging process on microstructure refining of semi-solid slurry of wrought aluminum alloy 7A09 [J]. Transactions of Nonferrous Metals Society of China, 2009, 19(Suppl.): 331−336.

[11] YI J, WANG G, LI S K, LIU Z W, GONG Y L. Effect of post-weld heat treatment on microstructure and mechanical properties of welded joints of 6061-T6 aluminum alloy [J]. Transactions of Nonferrous Metals Society of China, 2019, 29(10): 2035−2046.

[12] WANG W Y, PAN Q L, WANG X D, SUN Y W, YE J, LIN G, LIU S H, HUANG Z Q, XIANG S Q, WANG X P. Non-isothermal aging: A heat treatment method that simultaneously improves the mechanical properties and corrosion resistance of ultra-high strength Al−Zn−Mg−Cu alloy [J]. Journal of Alloys and Compounds, 2020, 845: 156286.

[13] ZHOU L, CHEN K H, CHEN S Y, DING Y F, FAN S M. Correlation between stress corrosion cracking resistance and grain- boundary precipitates of a new generation high Zn-containing 7056 aluminum alloy by non-isothermal aging and re-aging heat treatment [J]. Journal of Alloys and Compounds, 2021, 850: 156717.

[14] FENG D, ZHANG X M, LIU S D, WU Z Z, WANG T. Non-isothermal retrogression kinetics for grain boundary precipitate of 7A55 aluminum alloy [J]. Transactions of Nonferrous Metals Society of China, 2014, 24(7): 2122−2129.

[15] YOUSEFI M, JAMSHIDI AVAL H. Influence of rotational speed in friction surfacing of nickel−aluminide reinforced aluminum matrix composite on commercially pure aluminum [J]. Transactions of Nonferrous Metals Society of China, 2022, 32(8): 2480−2493.

[16] SEPEHRBAND P, WANG X, JIN H, ESMAEILI S. Microstructural evolution during non-isothermal annealing of a precipitation-hardenable aluminum alloy: Experiment and simulation [J]. Acta Materialia, 2015, 94: 111−123.

[17] BARDEL D, PEREZ M, NELIAS D, DESCHAMPS A, HUTCHINSON C R, MAISONNETTE D, CHAISE T, GARNIER J, BOURLIER F. Coupled precipitation and yield strength modelling for non-isothermal treatments of a 6061 aluminium alloy [J]. Acta Materialia, 2014, 62: 129−140.

[18] LIU H, CHEN Y, ZHAO G, LIU C M, ZUO L. Effect of pre-aging on precipitation behavior of Al−1.29Mg−1.22Si−0.68Cu−0.69Mn−0.3Fe−0.2Zn−0.1 Ti alloy [J]. Transactions of Nonferrous Metals Society of China, 2006, 16(4): 917−921.

[19] ZHAN X, TANG J G, LI H Z, LIANG X P, LU Y F, CHE Y X, TU W B, ZHANG Y D. Effects of non-isothermal aging on mechanical properties, corrosion behavior and microstructures of Al−Cu−Mg−Si alloy [J]. Journal of Alloys and Compounds, 2020, 819: 152960.

[20] LIU X Y, LI H W, ZHAN M, ZHANG H R. Quantitative characterization of lamellar α precipitation behavior of IMI834 Ti-alloy in isothermal and non-isothermal heat treatments [J]. Transactions of Nonferrous Metals Society of China, 2022, 32(1): 162−174.

[21] HU Z Y, FAN C H, SHEN T, OU L, DAI N S, WANG L. Effect of aging treatment on evolution of S' phase in rapid cold punched Al−Cu−Mg alloy [J]. Transactions of Nonferrous Metals Society of China, 2021, 31(7): 1930−1938.

[22] ZHANG J S, ZHONG X X, ZHANG L, WU G H, LIU W C. Effect of heat treatments on microstructure and mechanical properties of sand cast Al−2Li−2Cu−0.5Mg−0.2Sc−0.2Zr alloy [J]. Transactions of Nonferrous Metals Society of China, 2022, 32(2): 411−423.

[23] WENG Y Y, JIA Z H, DING L P, LIAO J, ZHANG P P, XU Y Q, LIU Q. Effect of pre-straining on structure and formation mechanism of precipitates in Al−Mg−Si−Cu alloy [J]. Transactions of Nonferrous Metals Society of China, 2022, 32(2): 436−447.

[24] KARTHIK G M, RAM G D J, KOTTADA R S. Friction stir selective alloying [J]. Materials Science and Engineering A, 2017, 684: 186−190.

[25] BARARPOUR S M, JAMSHIDI AVAL H, JAMAATI R. Mechanical alloying by friction surfacing process [J]. Materials Letters, 2019, 254: 394−397.

[26] PIRHAYATI P, JAMSHIDI AVAL H. Microstructural characterization and mechanical properties of friction surfaced AA2024−Ag composites [J]. Transactions of Nonferrous Metals Society of China, 2020, 30(7): 1756−1770.

[27] DILIP J J S, BABU S, RAJAN S V, RAFI K H, RAM G D J, STUCKER B E. Use of friction surfacing for additive manufacturing [J]. Materials and Manufacturing Processes, 2013, 28(2): 189−194.

[28] DILIP J J S, JANAKI RAM G D. Microstructure evolution in aluminum alloy AA 2014 during multi-layer friction deposition [J]. Materials Characterization, 2013, 86: 146−151.

[29] GANDRA J, VIGARINHO P, PEREIRA D, MIRANDA R M, VELHINHO A, VILAÇA P. Wear characterization of functionally graded Al−SiC composite coatings produced by friction surfacing [J]. Materials & Design, 2013, 52: 373−383.

[30] PIRHAYATI P, JAMSHIDI AVAL H, LOUREIRO A. Characterization of microstructure, corrosion, and tribological properties of a multilayered friction surfaced Al−Mg−Si−Ag alloy [J]. Archives of Civil and Mechanical Engineering, 2022, 22(4): 1−14.

[31] GANDRA J, KROHN H, MIRANDA R M, VILAÇA P, QUINTINO L, DOS SANTOS J F. Friction surfacing—A review [J]. Journal of Materials Processing Technology, 2014, 214(5): 1062−1093.

[32] SUHUDDIN U, MIRONOV S, KROHN H, BEYER M, DOS SANTOS J F. Microstructural evolution during friction surfacing of dissimilar aluminum alloys [J]. Metallurgical and Materials Transactions A, 2012, 43(13): 5224−5231.

[33] EHRICH J, ROOS A, KLUSEMANN B, HANKE S. Influence of Mg content in Al alloys on processing characteristics and dynamically recrystallized microstructure of friction surfacing deposits [J]. Materials Science and Engineering A, 2021, 819: 141407.

[34] HANKE S, DOS SANTOS J F. Comparative study of severe plastic deformation at elevated temperatures of two aluminium alloys during friction surfacing [J]. Journal of Materials Processing Technology, 2017, 247: 257−267.

[35] BIROL Y. The effect of sample preparation on the DSC analysis of 6061 alloy [J]. Journal of Materials Science, 2005, 40(24): 6357−6361.

[36] SALVO L, SUÉRY M. Effect of reinforcement on age hardening of cast 6061 Al□SiC and 6061 Al□Al_2O_3

particulate composites [J]. Materials Science and Engineering A, 1994, 177(1/2):19−28.

[37] DUTTA I, ALLEN S M. A calorimetric study of precipitation in commercial aluminium alloy 6061 [J]. Journal of Materials Science Letters, 1991, 10(6): 323−326.

[38] YANG X K, ZHANG L W, ZHANG S Y, LIU M, ZHOU K, MU X L. Properties degradation and atmospheric corrosion mechanism of 6061 aluminum alloy in industrial and marine atmosphere environments [J]. Materials and Corrosion, 2017, 68(5): 529−535.

非等温时效对含银 Al−Mg−Si 合金多层摩擦表面显微组织和腐蚀行为的影响

Hamed JAMSHIDI AVAL

Department of Materials Engineering, Babol Noshirvani University of Technology, Babol 47148-71167, Iran

摘　要：研究非等温时效对添加不同银含量 Al−Mg−Si 合金多层摩擦表面显微组织和腐蚀行为的影响。通过在耗材棒横截面上钻孔的方式添加 4%、8%和 13% (质量分数)的银。采用光学显微镜和电子显微镜研究涂层的显微组织，采用显微硬度和拉伸实验研究涂层的力学性能，采用电化学测试研究样品的耐腐蚀性。结果表明，随着银添加量从 4% (质量分数)增加到 13% (质量分数)，摩擦堆焊表面层的晶粒尺寸从(1.5±0.3) μm 减小到(1.0±0.3) μm。铝基体中的溶质银能够加速 Al−Mg−Si 合金的析出动力学。经非等温时效处理后，含银涂层的屈服强度和抗拉强度分别比不含银涂层高 50.6%和 43.5%。经非等温时效处理后，材料的腐蚀电流密度降低，含银和不含银样品的耐腐蚀性均提高，含银涂层的耐蚀性比无银镀层提高了 96.5%。

关键词：非等温时效；显微组织；腐蚀行为；Al−Mg−Si 合金；银添加剂；多层摩擦堆焊

(Edited by Wei-ping CHEN)